# Rapid synthesis process and characterization for high purity sodium thioantimoniate nonahydrate

Adam Bertrand, A. Paecklar, T. Barbier, F. Gascoin

ARTICLE

# Rapid Synthesis Process and Characterization for High Purity Sodium Thioantimoniate Nonahydrate

Received 00th January 20xx,
Accepted 00th January 20xx

DOI: 10.1039/x0xx00000x

A. Bertrand, [a] A. Paecklar, [a] T. Barbier,*[a] and F. Gascoin [a]

For the first time, $Na_3SbS_4.9H_2O$, also known as Schlippe's salt, has been synthesized through high-energy ball milling. This innovative synthesis way allows for obtaining high purity thioantimonate nonahydrate with around 90% yield in only approximately four hours. To validate the synthesis route described herein, the crystal structure has been refined, at room temperature, through high-resolution X-Ray diffraction, pair distribution function analysis and Energy Dispersive Spectrometry. Dehydration and rehydration of the compound have also been studied by thermogravimetric analysis and differential scanning calorimetry.

## Introduction

The limited Li resources in the Earth's crust, together with recent rapid rises in the price of the Li precursors, as well as its geologically uneven distribution are criteria that have to be taken into account for large-scale energy-storage applications.(1–3) Therefore, the replacement of $Li^+$ ions with $Na^+$ as charge carriers would be an ideal solution.

Thus, following that trend, sodium thioantimonates ($Na_3SbS_4$) and its conjugated nonahydrate ($Na_3SbS_4.9H_2O$), also known as Schlippe's salt, were highly studied for room-temperature-operable all-solid-state Na-ion batteries.(4–10) Indeed, sulfide Na-ion solid electrolytes are promising because of their potential for greater safety, lower cost, and performance compared to flammable organic liquid electrolytes used in Li-ion batteries.(11)

More recently, Schlippe's salt was used as antimony and sulfur precursors for hydrothermal synthesis of hybrid compounds.(12–14) The latter precursor, freely soluble in water compared to other classic antimony precursors, offers the great benefit of not using amine solvents, such as ethylenediamine, commonly used for dissolving sulfur compounds.(15) Therefore, such precursors allow obtaining of ternary and quaternary sulfide compounds by eliminating the use of toxic solvents and the production of hazardous waste. However, the salt is no longer available for commercial purchase, which means it is now necessary to synthesize it efficiently and quickly for it to not become too much of a time cost on processes where this compound is needed. Unfortunately, most synthesis methods reported recently are multiple days long due to the slow recrystallization process and have a low yield of approximately 30%.(13)

Herein, a new rapid and scalable synthesis method, using high-energy ball-milling, is described for the first time. This process, which allows obtaining single-phase compounds in only four hours possesses the great benefits of no concerns about the generation of toxic $H_2S$ gas or other noxious process intermediates.

To attest to the innovative method used for synthesizing single-phase sodium thioantimoniate nonahydrate, structural characterization performed through X-Ray diffraction and pair distribution function analysis have been performed. The crystallographic parameters have then been compared and discussed with the ones previously reported.(16)

## Experimental section

A mixture of binary $Na_2S$ (Alpha Aesar, 97%, 1.93 g, 24.7 mmol), $Sb_2S_3$ (Sigma-Aldrich, 98%, 2.82 g, 8.26 mmol), and elemental S (Alpha Aesar, 99,5%, 0.533 g, 16.6 mmol) was introduced, into 9 mL of distilled water inside a 45 mL tungsten carbide jar containing 48 tungsten carbide balls with a diameter of 5 mm (49.7 g). The mixture was then milled at 450 rpm for 2 hours (divided into 8 cycles of 15 minutes, each separated with a minute-long break to let the system cool down). The resulting solution was washed and filtered with deionized water. The dark brown powder obtained of unwanted products ($Na_2SO_4$ and $Sb_2O_3$) was discarded. The filtrate was dried through rotary

[a] CRISMAT, UMR6508 CNRS ENSICAEN, 6 bd Maréchal Juin, 14050 CAEN cedex 4, France. Email : Tristan.barbier@ensicaen.fr

† Footnotes relating to the title and/or authors should appear here.

Electronic Supplementary Information (ESI) available: [details of any supplementary information available should be included here]. See DOI: 10.1039/x0xx00000x

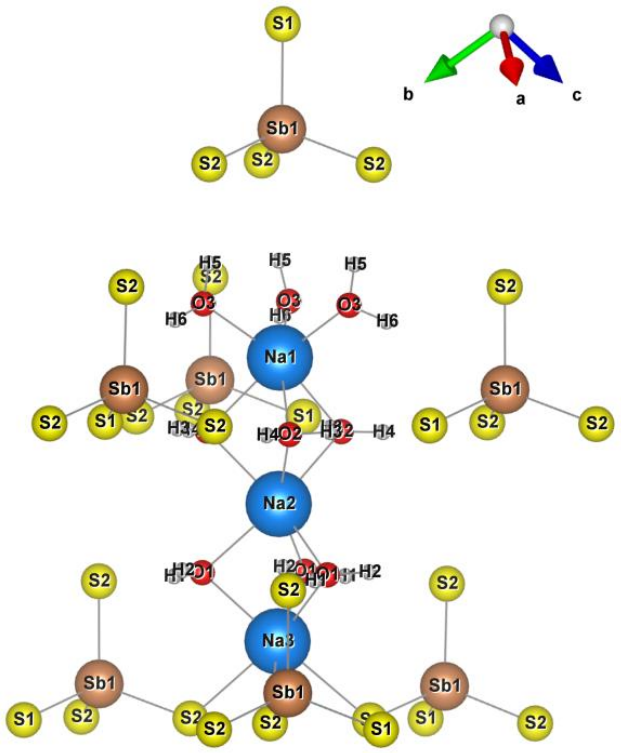


**Figure 1:** Schlippe's salt structure along a Na1-Na2-Na3 axis.

evaporation to force the salt's precipitation. The powder obtained was then recovered and characterized.

The crystallographic parameters were determined through high-resolution powder X-Ray Diffraction (XRD). The data were collected at room temperature with two different devices. First, through a Bruker D8 ADVANCE diffractometer [copper anode λ = 1.54059 Å, monochromatic Ge 111, Lynx Eye detector], in reflection configuration. Data were collected from 8 up to 100° with a step size of 0.009198°, and a step time of 1.7 s. A diffraction pattern of a standard $LaB_6$ powder was also registered under the same conditions to obtain the instrumental broadening of the diffractometer. The peak shape was then corrected from the instrumental broadening using the aforementioned calibration acquisition. Those data were then refined using the FullProf and WinPlotr software package.(17,18)

Regarding the structure refinement, the systematic error correction (zero-point shift and asymmetry) was applied, and the background was adjusted using a polynomial function. With respect to the crystallographic structure, the lattice parameters, atomic positions, and isothermal temperature factor ($B_{iso}$) were also refined. Hydrogen atoms, however, have been set with the parameters that were already determined by K. Mereiter *et al.* (16) through neutron diffraction. Indeed, the fact that hydrogen atoms only have one electron makes them very hard to detect with X-Rays accurately due to X-Rays' scatter from the electron density. (19,20)

Secondly, X-Ray scattering data suitable for Pair Distribution Function (PDF) analysis were collected using a Rigaku SmartLab (rotating anode Mo λ = 0.71146 Å) diffractometer. The

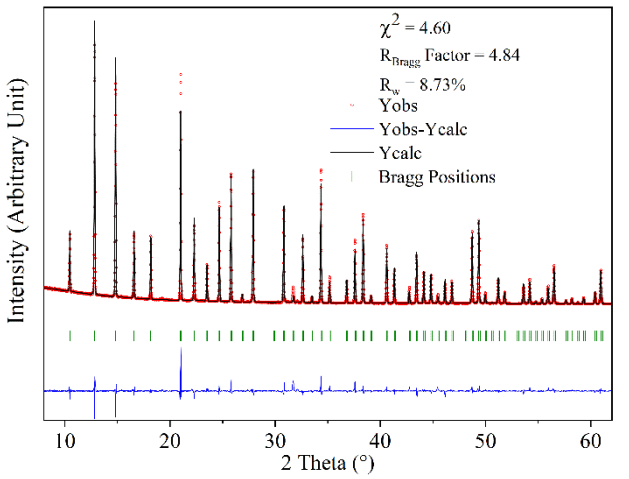


**Figure 2**: powder X-Ray diffraction patterns of Schlippe's Salt with D8 ADVANCE.

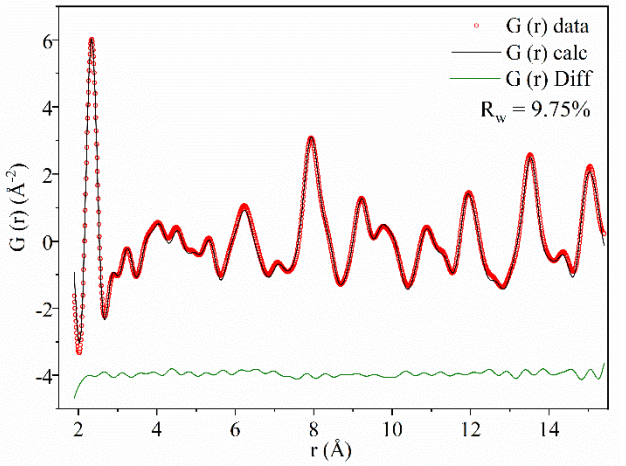


**Figure 3:** PDF refinement of Schlippe's Salt with Smartlab Rigaku.

powdered sample was loaded into a quartz capillary (0.4 mm in diameter) and measured in transmission mode using a HyPix3000 detector. Data were collected from 3 to 112° using four different speed-time, depending on the angular range (3° to 35°: 4 °/min; 34° to 65°: 1.5 °/min; 64° to 95°: 0.7 °/min, and 94° to 112°: 0.2 °/min). The experimental PDF was extracted using the program PDFgetX3 (21) and analyzed using the program PDFgui.(22) The total scattering structure-function, *S(Q)*, was produced in PDFgetX3 by subtracting the quartz container scattering and utilizing the appropriate sample composition. The pair distribution function pattern, *G(r)*, displayed in figure 3, was calculated via the Fourier transform of the total scattering data utilizing a maximum $Q_{MaxInst}$ = 14.6431 Å$^{-1}$. Values of $Q_{damp}$ = 0.02 Å$^{-1}$ and $Q_{broad}$ = 0.08 Å$^{-1}$ have been extracted from the refinement of a $LaB_6$ standard in PDFgui software and were used for further refinement.(22)

Imaging, mapping, and elemental analysis were performed using a Scanning Electron Microscope (SEM; JEOL - JCM7000) equipped with an Energy Dispersive Spectrometer (EDS). The samples were measured at an operating voltage of 15 kV.

The study of water inside the crystal structure was performed through Thermo-Gravimetric Analysis (TGA). The data was collected on a Netzsch TGA apparatus (STA 449 F3 Jupiter) over

the temperature range of 300 °C with 3 °C/min. An $N_2$ flux (100 mL/min) and air ($N_2$ 80 mL/min - $O_2$ 20 mL/min) were used during the acquisition.

## Results and discussion

### Structural analysis

This new rapid and scalable synthesis method presented herein resulted in a satisfying yield of around 90% in mass for only a four hours long process, which is far higher than the 30% yield obtained by a multiple-day-long protocol of dissolution, precipitation, and recrystallization.(13) As varying traces of the mopungite phase ($NaSb(OH)_6$) can appear during the process due to the decomposition under light (12), it is recommended to use the least amount of water possible during washing and have a powerful vacuum for the process to be done as fast as possible.

The room temperature XRD pattern of Schlippe's Salt obtained from the Bruker D8 ADVANCE diffractometer is shown in Figure 2. The one obtained through the Rigaku SmartLab diffractometer is shown in Figure 3.

The devices' attributes used, as well as the unit cell characteristics, determined with these patterns, are reported in Table 1.

Atomic positions and isotropic displacement parameters, obtained from the refinement of the D8 ADVANCE pattern, are reported in Table 2.

It will be noted that atomic positions and isotropic displacement parameters of hydrogen atoms have been set (all $B_{Iso}$ being considered at 3.2 Å$^2$) and the refinement of oxygen parameters have been processed with distances set to 0.9584 Å and a standard error allowed of 0.0020 Å while angles in the water structure were set to 106.45° with a standard error: 2.0000° (these settings were based on water molecules parameters(23) and following the decisions made by Mereiter *et al.*(16)). Refinements without these constraints have led to non-physical results (abnormal distances and angles for water molecules) from the software with little improvement on the reliability factors such as the R-Factor.

**Table 1:** Crystal data for Schlippe's Salt at 293K.

| *Chemical Formula* | $Na_3SbS_4.9H_2O$ | |
|---|---|---|
| *Molecular weight (g/mol)* | 481.12 | |
| *Space Group* | P $2_1$ 3 (198) | |
| *Refinement* | Rietveld (D8 ADVANCE) | PDF (Rigaku Smartlab) |
| *Radiation* | Cu 1.54059 Å | Mo 0.71146 Å |
| *Cell Parameters* | | |
| *a (Å)* | 11.959(2) | 11.966(8) |
| *α (°)* | 90° | 90° |
| *V (Å$^3$)* | 1710.438(5) | 1713.710(1) |
| *Calculated density (g/cm$^3$)* | 1.868 | 1.864 |

**Table 2:** Atomic coordinates and isotropic displacement parameters ($B_{Iso}$) obtained from D8 diffractometer (* are fixed atoms).

| *Atom* | *x* | *y* | *z* | $B_{Iso}$ (Å$^2$) |
|---|---|---|---|---|
| ***Na1*** | 0.2893(4) | 0.2893(4) | 0.2893(4) | 3.6932(9) |
| ***Na2*** | 0.4512(2) | 0.4512(2) | 0.4512(2) | 2.9442(3) |
| ***Na3*** | 0.6031(3) | 0.6031(3) | 0.6031(3) | 4.7133(1) |
| ***Sb*** | 0.0366(3) | 0.0366(3) | 0.0366(3) | 2.1683(5) |
| ***S1*** | 0.9205(3) | 0.9205(3) | 0.9205(2) | 2.6582(2) |
| ***S2*** | 0.1521(1) | 0.1479(2) | 0.9230(2) | 2.3399(8) |
| ***O1*** | 0.9748(1) | 0.3673(6) | 0.9245(7) | 1.6732(1) |
| ***O2*** | 0.1826(1) | 0.6950(4) | 0.9937(3) | 1.6392(3) |
| ***O3*** | 0.1028(6) | 0.2602(2) | 0.3252(4) | 2.5602(4) |
| ***H1**** | 0.0246(1) | 0.3049(1) | 0.9276(0) | 3.2 |
| ***H2**** | 0.9280(9) | 0.3598(1) | 0.8602(0) | 3.2 |
| ***H3**** | 0.2515(1) | 0.6614(1) | 0.0193(0) | 3.2 |
| ***H4**** | 0.1665(1) | 0.7573(1) | 0.0405(0) | 3.2 |
| ***H5**** | 0.0553(1) | 0.2304(1) | 0.2681(0) | 3.2 |
| ***H6**** | 0.0593(1) | 0.3107(1) | 0.3702(0) | 3.2 |

**Table 3**: Atomic coordinates and isotropic displacement parameters ($B_{Iso}$) obtained from the Rigaku Smartlab diffractometer (* are fixed atoms).

| *Atom* | *x* | *y* | *z* | $B_{Iso}$ (Å$^2$) |
|---|---|---|---|---|
| ***Na1*** | 0.2892(9) | 0.2892(9) | 0.2892(9) | 6.2798(7) |
| ***Na2*** | 0.4424(3) | 0.4424(3) | 0.4424(3) | 1.1511(9) |
| ***Na3*** | 0.5951(9) | 0.5951(9) | 0.5951(9) | 2.0016(6) |
| ***Sb*** | 0.0363(3) | 0.0363(3) | 0.0363(3) | 1.2064(6) |
| ***S1*** | 0.9236(4) | 0.9236(4) | 0.9236(4) | 0.7381(6) |
| ***S2*** | 0.1485(7) | 0.1401(5) | 0.9241(7) | 1.9186(5) |
| ***O1*** | 0.9781(3) | 0.3477(5) | 0.9283(1) | 0.9209(5) |
| ***O2*** | 0.1640(1) | 0.6965(6) | 0.9923(4) | 0.7658(8) |
| ***O3*** | 0.0941(5) | 0.2395(5) | 0.3292(7) | 2.0694(5) |
| ***H1**** | 0.0246(1) | 0.3049(1) | 0.9276(1) | 3.2 |
| ***H2**** | 0.9280(9) | 0.3598(1) | 0.8602(1) | 3.2 |
| ***H3**** | 0.2515(1) | 0.6614(1) | 0.0193(1) | 3.2 |
| ***H4**** | 0.1665(1) | 0.7573(1) | 0.0405(1) | 3.2 |
| ***H5**** | 0.0553(1) | 0.2304(1) | 0.2681(1) | 3.2 |
| ***H6**** | 0.0593(1) | 0.3107(1) | 0.3702(1) | 3.2 |

Atomic positions obtained from the PDF refinement of the Rigaku SmartLab pattern are reported in Table 3.

Both X-Ray and PDF refinements were performed using the $P2_13$ space group (198). All peaks have been adequately considered (as it can be seen in Figures 2 & 3), and no extra peaks may be observed over the full angular range, thus confirming the high purity of the sample.

When comparing results, our crystallographic parameters are quite similar to those previously reported.(16)

Indeed, the *a* cell parameter obtained through X-Ray diffraction and PDF refinement, 11.959(2) Å and 11.966(8) Å respectively, are very similar to those reported by K. Mereiter *et al.* (11.957(3) Å) and S. Haussühl *et al.* (11.957(2) Å). (16,24)

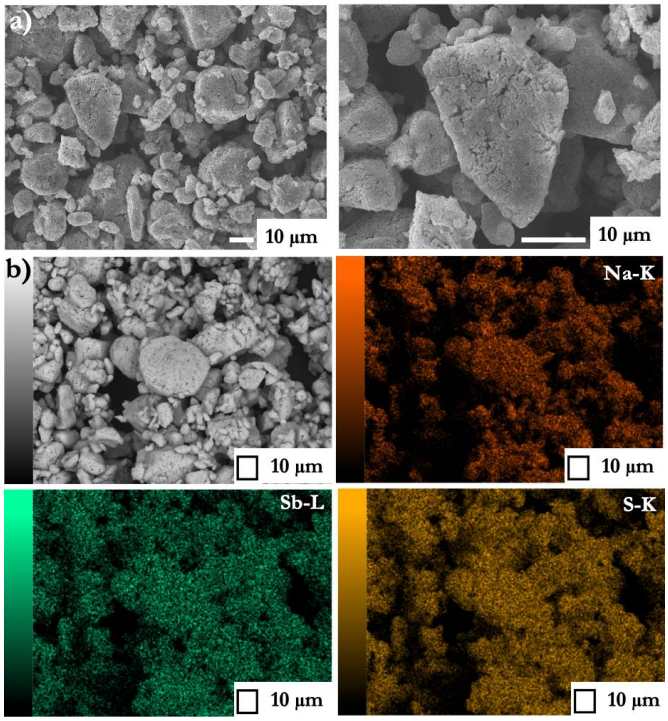


**Figure 4:** SEM images a) with x1000 and x2500 magnification b) with EDS-Elemental mapping of Na, Sb and S.

The deduced values confirm once again the high purity of the sample as well as the water amount because the dehydrated compound ($Na_3SbS_4$) crystallizes in the $P\bar{4}2_1c$ space group (a = 7.1653 Å). (25)

Just as cell parameters, atomic coordinates of all atoms (despite hydrogen) have also been compared to those obtained through X-Ray and neutron diffraction, previously published by K. Mereiter *et al.* Apart from the coordinates of the H atoms, the X-Ray results are more precise for Na, Sb, and S than the neutron results, and nearly as precise for the O atoms. Thus, the relative distances between the published data and those obtained from X-Ray diffraction (this study) highlight very similar coordinates.

Indeed, the biggest difference, which may be observed for the $yO_3$ position is around 0.43%.

As aforementioned, light element analysis is notoriously challenging because of the small number of form factors light elements generate which may explain the lowest accuracy provided by the X-Ray diffraction technique regarding the oxygen atoms.

On another hand, atomic coordinates deduced from the PDF refinement also exhibit similar values for the heavy atoms while slight deviations may be observed for the oxygen ones. It might also be pointed out that no constraints were applied to set the distance (and angle) of the water molecules. Therefore, the highest relative gap between the coordinates might be observed for $yO_1$ (1.87% deviation), $xO_2$ (2.00% deviation), and $yO_3$ (1.64 % deviation).

### Elemental composition

As SEM analysis shows in figure 4.a), particles formed through this synthesis method average at 12.4 µm with a range between 2 and 33 µm. The particles themselves appear to be quite porous. Additionally, EDS allows checking of the elemental composition to ensure its homogeneity, as presented in figure 4.b), and estimate the proportions of sodium, antimony, and sulfur present in these particles.

On average, it was estimated that experimental composition was of 36%, 14%, and 50% which is rather close compared to the 37.5%, 12.5%, and 50% expected in theory for Na, Sb, and S respectively.

### Dehydration

TGA results are shown in Figures 5 and 6, where each horizontal line represents the number of water molecules present in the structure (9 at 100%, 0 at 66.16%). From those results, it can be determined that water in the structure evaporates as soon as 30°C up to approximately 100°C in both tests. Differences are visible at approximately 200°C where, while the powder stays unchanged under $N_2$, oxidation clearly happens under air. The

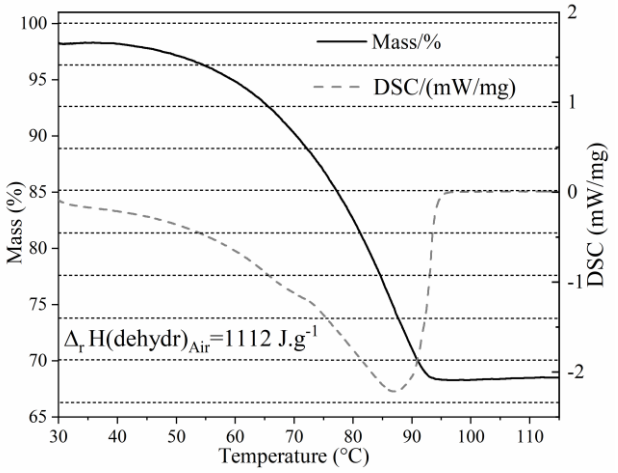


**Figure 5:** DSC-TGA curves of Schlippe's Salt in air. Heating rate = 3 °C/min.

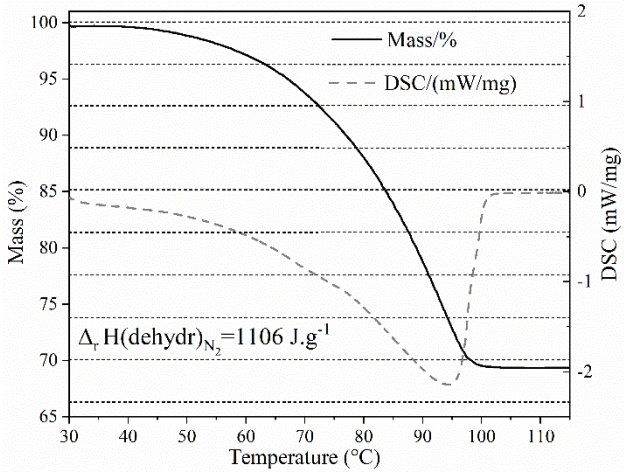


**Figure 6:** DSC-TGA curves of Schlippe's Salt in nitrogen. Heating rate = 3 °C/min.

compounds formed are $Sb_2S_3$, $Sb_2O_3$, and $Na_2SO_4$. In the case of the dehydrated compound, it rapidly reabsorbs water from ambient air and returns to its original $Na_3SbS_4 \cdot 9H_2O$ composition. The experimental value of enthalpy of the dehydration process can be calculated from DSC. Both values obtained are rather close, (-1106 $J \cdot g^{-1}$ and -1112 $J \cdot g^{-1}$). However, it can be noticed that not all the water is exactly extracted from the compound. It could be assumed that the leftover water is the last molecule still maintaining Schlippe's Salt structure before a rearrangement into the anhydrous compound as other works already show that the formation of $Na_3SbS_4$ is more complicated than a simple heating of its hydrated form.(4)

## Conclusions

Here, a fast and highly efficient synthesis process of Schlippe's Salt was described. Using a ball mill and rotary evaporator in order to bring the energy for a complete reaction and a fast recovery of the compound to guarantee its high purity. The method has proved to be more efficient than those used so far for the synthesis of this compound since it is no longer available for commercial purchase.

The compound has also been characterized with X-Ray diffraction, coupled with pair distribution function analysis to assess its crystal structure. Both methods lead to similar results and concur with those that can be found in the literature. A brief exploration of the salt's behaviour under heating with thermogravimetric analysis and differential scanning calorimetry shows that the salt decomposes under air and stays stable under nitrogen. However, it is difficult to fully extract the remaining water present in the structure.

## Conflicts of interest

There are no conflicts of interest to declare.

## Acknowledgements


- The authors acknowledge the financial support provided by the ANR LISBON (ANR-20-CE05-0022-01) project and the Normandy region.
- The authors would like to thank the ENSICAEN engineering school and staff for providing the rotary evaporator


## Notes and references


1. Kalhoff J, Eshetu GG, Bresser D, Passerini S. Safer Electrolytes for Lithium-Ion Batteries: State of the Art and Perspectives. ChemSusChem. 2015 Jul 8;8(13):2154–75.

2. Manthiram A, Yu X, Wang S. Lithium battery chemistries enabled by solid-state electrolytes. Nat Rev Mater. 2017 Apr;2(4):16103.

3. Yabuuchi N, Kubota K, Dahbi M, Komaba S. Research Development on Sodium-Ion Batteries. Chem Rev. 2014 Dec 10;114(23):11636–82.

4. Banerjee A, Park KH, Heo JW, Nam YJ, Moon CK, Oh SM, et al. Na $_3$ SbS $_4$ : A Solution Processable Sodium Superionic Conductor for All-Solid-State Sodium-Ion Batteries. Angew Chem Int Ed. 2016 Aug 8;55(33):9634–8.

5. Jalem R, Gao B, Tian HK, Tateyama Y. Theoretical study on stability and ion transport property with halide doping of Na 3 SbS 4 electrolyte for all-solid-state batteries. J Mater Chem A. 2022;10(5):2235–48.

6. Shimoda M, Maegawa M, Yoshida S, Akamatsu H, Hayashi K, Gorai P, et al. Controlling Defects to Achieve Reproducibly High Ionic Conductivity in Na3SbS4 Solid Electrolytes. Chem Mater [Internet]. 2022 Jun 6 [cited 2022 Jun 27]; Available from: https://doi.org/10.1021/acs.chemmater.2c00944

7. Won Kim T, Ho Park K, Eun Choi Y, Yeon Lee J, Seok Jung Y. Aqueous-solution synthesis of Na 3 SbS 4 solid electrolytes for all-solid-state Na-ion batteries. J Mater Chem A. 2018;6(3):840–4.

8. Zhang J. Synthesis via an organic molten salt solvent route and characterization of PbS nanocrystals. Cryst Res Technol. 2011 Oct;46(10):1058–64.

9. Jalem R, Hayashi A, Tsuji F, Sakuda A, Tateyama Y. First-Principles Calculation Study of Na+ Superionic Conduction Mechanism in W- and Mo-Doped Na3SbS4 Solid Electrolytes. Chem Mater. 2020 Oct 13;32(19):8373–81.

10. Rush LE, Hood ZD, Holzwarth NAW. Unraveling the electrolyte properties of ${\mathrm{Na}}_{3}{\mathrm{SbS}}_{4}$ through computation and experiment. Phys Rev Mater. 2017 Dec 11;1(7):075405.

11. Zhao C, Liu L, Qi X, Lu Y, Wu F, Zhao J, et al. Solid-State Sodium Batteries. Adv Energy Mater. 2018;8(17):1703012.

12. Anderer C, Delwa de Alarcón N, Näther C, Bensch W. A Strategy for the Preparation of Thioantimonates Based on the Concept of Weak Acids and Corresponding Strong Bases. Chem - Eur J. 2014 Dec 15;20(51):16953–9.

13. Danker F, Engesser TA, Broich D, Näther C, Bensch W. The cation and anion bonding modes make a difference: an unprecedented layered structure and a tri(hetero)nuclear moiety in thioantimonates( v ). Dalton Trans. 2021;50(48):18107–17.

14. Danker F, Anderer C, Poschmann M, Terraschke H, Näther C, van Leusen J, et al. [Mn(terpy)Sb2S4]n, a 1D Network of MnSb4S5 Rings Exhibiting a Pronounced Magnetocaloric Effect and Luminescence. Eur J Inorg Chem. 2020;2020(18):1751–8.

15. Zotov A, Shikina ND, Akinfiev N. Thermodynamic properties of the Sb(III) hydroxide complex Sb(OH)3(aq) at hydrothermal conditions. 2003;

16. Mereiter K, Preisinger A, Guth H. Hydrogen bonds in Schlippe's salt: refinement of the crystal structures of Na3SbS4.9H2O by X-ray diffraction and Na3SbS4.9D2O by neutron diffraction at room temperature. Acta Crystallogr B. 1979 Jan 15;35(1):19–25.

17. Rodríguez-Carvajal J. Recent advances in magnetic structure determination by neutron powder diffraction. Phys B Condens Matter. 1993 Oct;192(1–2):55–69.

18. Roisnel T, Rodríquez-Carvajal J. WinPLOTR: A Windows Tool for Powder Diffraction Pattern Analysis. Mater Sci Forum. 2001 Oct;378–381:118–23.

19. Schmidtmann M, Coster P, Henry PF, Ting VP, Weller MT, Wilson CC. Determining hydrogen positions in crystal engineered organic molecular complexes by joint neutron powder and single crystal X-ray diffraction. CrystEngComm. 2014 Jan 23;16(7):1232–6.

20. Müller P, Herbst-Irmer R, Spek AL, Schneider TR, Sawaya MR. Crystal Structure Refinement: A Crystallographer's Guide to SHELXL [Internet]. Oxford: Oxford University Press; 2006 [cited 2022 Apr 28]. 232 p. (International Union of Crystallography Texts on Crystallography). Available from: https://oxford.universitypressscholarship.com/10.1093/acprof:oso/9780198570769.001.0001/acprof-9780198570769

21. Juhás P, Davis T, Farrow CL, Billinge SJL. *PDFgetX3* : a rapid and highly automatable program for processing powder diffraction data into total scattering pair distribution functions. J Appl Crystallogr. 2013 Apr 1;46(2):560–6.

22. Farrow CL, Juhas P, Liu JW, Bryndin D, Božin ES, Bloch J, et al. PDFfit2 and PDFgui: computer programs for studying nanostructure in crystals. J Phys Condens Matter. 2007 Aug 22;19(33):335219.

23. Hoy AR, Bunker PR. A precise solution of the rotation bending Schrödinger equation for a triatomic molecule with application to the water molecule. J Mol Spectrosc. 1979 Jan 1;74(1):1–8.

24. Haussühl S. Isotopie-Effekte in den optischen, elektrischen, elastischen und thermischen Eigenschaften der Schlippeschen Salze Na3SbS4 · 9H2O und Na3SbS4 · 9D2O. Z Für Krist - Cryst Mater. 1970 Dec 1;132(1–6):255–65.

25. Gamo H, Phuc NHH, Muto H, Matsuda A. Effects of Substituting S with Cl on the Structural and Electrochemical Characteristics of Na3SbS4 Solid Electrolytes. ACS Appl Energy Mater. 2021 Jun 28;4(6):6125–34.

 